5-28-2019

Molecular oxygen generation from the reaction of water cations with oxygen atoms

Ryan C. Fortenberry
University of Mississippi

Tarek Trabelsi
University of Pennsylvania

Brent R. Westbrook
St. Edward's University

Weston A. Del Rio
University of Mississippi

Joseph S. Francisco
University of Pennsylvania

Ryan C. Fortenberry, Tarek Trabelsi, Brent R. Westbrook, Weston A. Del Rio, and Joseph S. Francisco

View Online   **Export Citation**   **CrossMark**

ARTICLES YOU MAY BE INTERESTED IN

Molecular oxygen generation from the reaction of water cations with oxygen atoms

View Online   Export Citation   CrossMark

Ryan C. Fortenberry,[1,a)] Tarek Trabelsi,[2] Brent R. Westbrook,[3] Weston A. Del Rio,[1]
and Joseph S. Francisco[2]

AFFILIATIONS

[1] Department of Chemistry and Biochemistry, University of Mississippi, University, Mississippi 38677-1848, USA
[2] Department of Earth and Environmental Science Philadelphia, University of Pennsylvania, Philadelphia, Pennsylvania 19104, USA
[3] Department of Chemistry, St. Edward's University, Austin, Texas 78704, USA

[a)] r410@olemiss.edu

ABSTRACT

The oxywater cation (H_2OO^+), previously shown to form barrierlessly in the gas phase from water cations and atomic oxygen, is proposed here potentially to possess a $^2A'' \leftarrow {}^4A''$ excitation leading to the $H_2 \cdots O_2^+$ complex. This complex could then easily decompose into molecular hydrogen and the molecular oxygen cation. The present quantum chemical study shows that the necessary electronic transition takes place in the range of 1.92 eV (645 nm), in the orange-red range of the visible and solar spectrum, and dissociation of the complex only requires 5.8 kcal/mol (0.25 eV). Such a process for the abiotic, gas phase formation of O_2 would only need to be photocatalyzed by visible wavelength photons. Hence, such a process could produce O_2 at the mesosphere/stratosphere boundary as climate change is driving more water into the upper atmosphere, in the comet 67P/Churyumov-Gerasimenko where surprisingly high levels of O_2 have been observed, or at gas-surface (ice) interfaces.

Published under license by AIP Publishing. https://doi.org/10.1063/1.5102073

INTRODUCTION

Recent work has shown that, in the gas phase, water will form bonds originating on the oxygen atom with every atomic cation from hydrogen even to argon.[1] Quintessentially, hydronium (H_3O^+) is a pillar of acid-base chemistry and has even been observed in the interstellar medium (ISM).[2] More interesting, though, the bonding of water cation with atomic oxygen is shown to be stable in forming the oxywater cation. In this molecule, the O–O bond energy is 54.08 kcal/mol[1] which is notably greater than that of hydrogen peroxide with a O–O bond energy of a meager 33.9 kcal/mol, enough to be cleaved by sunlight. However, this present work will discuss a previously unreported quaternary minimum.

RESULTS AND DISCUSSION

The creation of the oxywater cation (H_2OO^+)[3–5] from water cations and atomic oxygen progresses barrierlessly through a wide minimum for the association of $O(^3P)$ to H_2O^+ potential energy surface (PES), shown in the green ($1^4A''$) line of Fig. 1 and previously demonstrated by Ref. 1. Then, electronic emission can create the doublet surface(s) (magenta X^2A' and red $1^2A''$ lines of Fig. 1) where the molecule can relax into its optimized and stable minimum. In such a process, the resulting vibrational cascade would be reduced since the doublet surface crosses the quartet surface nearly at its minimum making the bonding reaction much faster than is typical of radiative association reactions which are notoriously slow. Consequently, these CCSD(T)-F12/cc-pVTZ-F12 computations[6,7] show that not only is the oxywater cation stable, but it should also form relatively easily.[1] These computations have also been verified with multireference configuration interaction theory via MRCISD(+Q)/aug-cc-pVTZ computations[8,9] giving the same potential energy curves as provided in Fig. S1 of the supplementary material. Furthermore, these MRCI computations clearly show that formation of H_2OO^+ in this process likely is initiated with H_2O^+ and oxygen atoms. Formation through the alternate $O^+(^3S)$ and H_2O channel does not appear to couple with these low-lying states. Further work will explore this pathway.
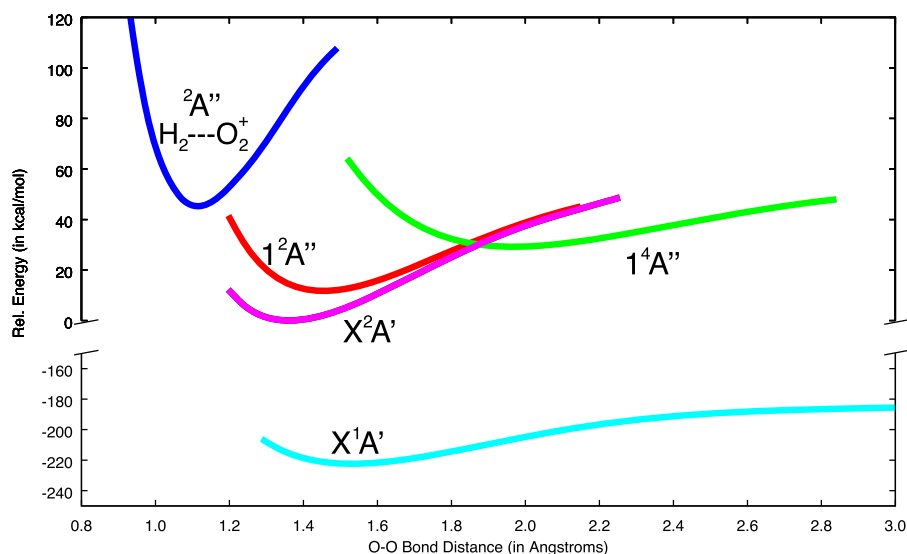
FIG. 1. The CCSD(T)-F12/cc-pVTZ-F12 one-dimensional potential energy surface (in kcal/mol) for the O–O stretch of H_2OO^+. Curves: cyan, $^1A'$ H_2OO; magenta, X^2A' H_2OO^+; red, $1^2A''$ H_2OO^+; green, $1^4A''$ H_2OO^+; and blue, $^2A''$ $H_2\cdots O_2^+$.

The oxywater neutral will break apart more easily since the O–O bond dissociation energy is on the order of 40 kcal/mol (cyan X^1A' line in Fig. 1). The ionization potential of H_2OO is computed here to be 9.58 eV, significantly more than the O–O bond energy as observed in Fig. 1 where the magenta X^2A' line is well above the cyan X^1A' asymptotic dissociation limit. Furthermore, there do not appear to be any other states that interact with the ground state of H_2OO. The oxywater cation, on the other hand, is more likely to engage in novel chemistry. Most notably, H_2OO^+ has another state of interest that gives many indications of leading to molecular oxygen.

The blue line in Fig. 1 represents a $^2A''$ electronically excited state of a H_2OO^+ that ultimately gives rise to the $H_2\cdots O_2^+$ complex, H_2 weakly bound to O_2^+. The ionization potential of O_2 is notably less than H_2 (12.07 eV vs 15.43 eV)[10] likely forbidding the formation of the $O_2\cdots H_2^+$ system. Present CCSD(T)-F12/cc-pVTZ-F12 computations predict the optimized O–O bond length in this molecular complex to be 1.117 Å which is nearly exactly that for O_2^+ at 1.116 Å from the experiment,[10] putting the positive charge on the oxygen molecule portion. Additionally, with X defined as the center-of-mass in the H_2 portion, the optimized X–H value is 0.374 Å making H–H 0.748 Å, close to the experimental 0.741 Å for H_2.[10] The rest of the geometric parameters for $H_2\cdots O_2^+$, as well as the doublet and quartet forms of H_2OO^+ for comparison, are given in Table I.

The $^2A''$ $H_2\cdots O_2^+$ complex lies adiabatically 39.3 kcal/mol (1.70 eV) above the X^2A' ground state of H_2OO^+ and only a mere 12.6 kcal/mol (0.54 eV) above the $1^4A''$ state. The binding of the oxygen molecular cation to the hydrogen molecule in $H_2\cdots O_2^+$ is computed here to be 5.8 kcal/mol from a simple products minus reactants model. While the O–X distance gives a fairly flat potential, the $\angle$O–O–X angle is more rigid at the optimized 111.5° similar to ligands of NO^+.[11]

As shown in Fig. 2, the electronic states of H_2OO^+ and that from the $H_2\cdots O_2^+$ complex have different orbital occupations, but the topologies of the orbitals themselves largely remain consistent. The ground X^2A' state of the oxywater cation has a $(\text{core})(3a')^2(4a')^2(1a'')^2(5a')^2(6a')^2(2a'')^2(7a')$ orbital occupation. The other doublet ($1^2A''$, red line in Fig. 1) excites one electron from the $2a''$ orbital into the $7a'$, as shown in Fig. 3. The $1^4A''$ state excites one electron from the same $2a''$ orbital in the ground X^2A' state of H_2OO^+ into a higher $8a'$ in the third column in Fig. 3. These three orbitals in this active space represent the three antibonding p orbital combinations from the oxygen atoms: $2a''$ being π_y^*, $7a'$ being the π_z^* highest-occupied molecular orbital (HOMO), and $8a'$ being the σ^* lowest-unoccupied molecular orbital (LUMO). These are visually depicted in Figs. 2(a)–2(c), respectively.

The $^2A''$ $H_2\cdots O_2^+$ complex occupation is defined as $(\text{core})(3a')^2(4a')^2(1a'')^2(5a')^2(6a')^2(7a')^2(2a'')$ and is compared to the other states' occupations in the last column of Fig. 3. Hence, the $^2A''$ $H_2\cdots O_2^+$ state and the ground X^2A' state of H_2OO^+ have the same occupation of the same orbitals up to the HOMO-2 $6a'$ orbital. These are mostly the expected O_2 MOs for the first six levels. The actual HOMO-1, HOMO, and LUMO for this complex are all shown in Figs. 2(d)–2(f). In this complex, $7a'$ HOMO-1 is the H–H σ bond, the $2a''$ HOMO is the π_y^*, and the $8a'$ LUMO is the π_z^*.

TABLE I. The CCSD(T)-F12/cc-pVTZ-F12 optimized geometries.[a]

	X^2A' H_2OO^+	$1^4A''$ H_2OO^+	$^2A''$ $H_2\cdots O_2^+$
O–O (Å)	1.362	1.964	1.117
X–H (Å)	0.846	0.791	0.374
O–X (Å)	0.507	0.578	2.424
$\angle$O–O–X (deg)	137.4	112.9	111.5

[a]X represents the center-of-mass in the H_2 moiety, i.e., half of the H–H bond length. This parameter gives more generic coordinates between the two isomers.
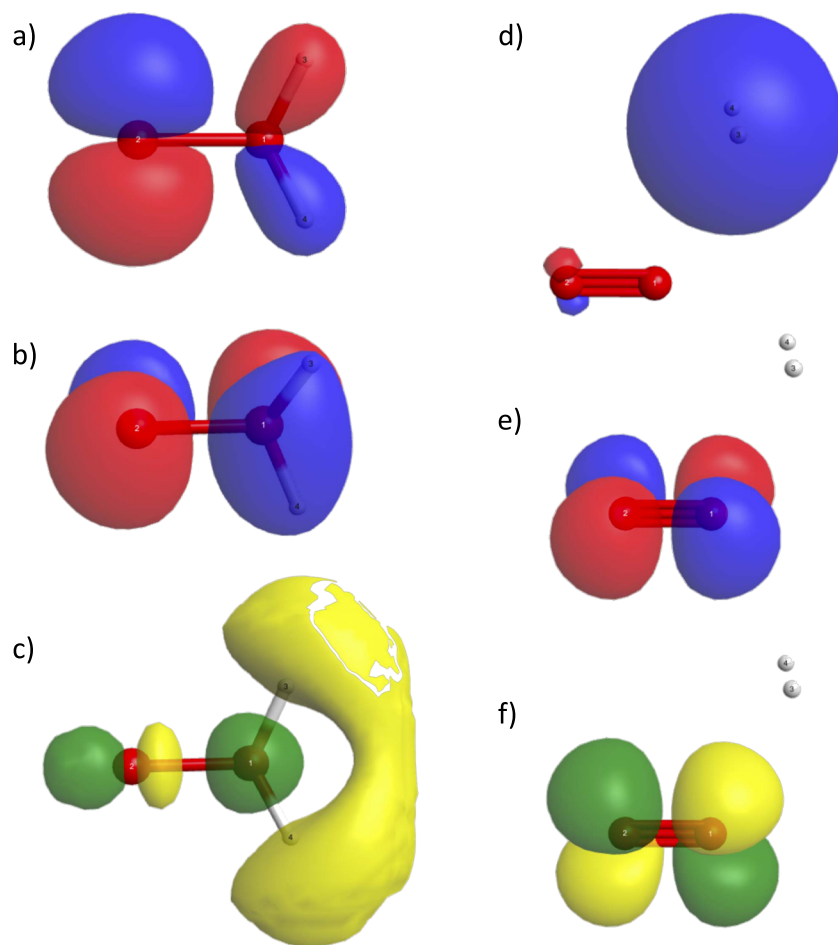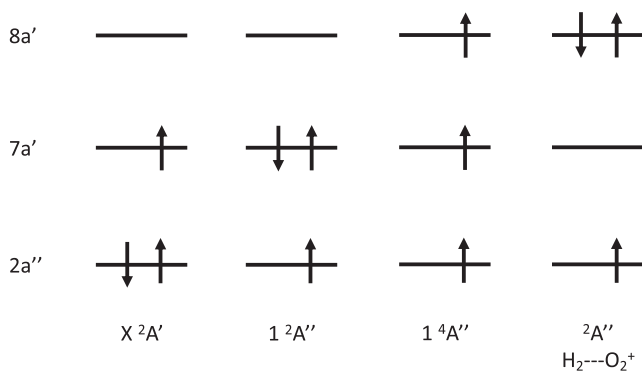
FIG. 2. The H_2OO^+ MOs: (a) $2a''$ HOMO-1, (b) $7a'$ HOMO, and (c) $8a'$ LUMO; as well as the $H_2 \cdots O_2^+$ MOs: (d) $7a'$ HOMO-1, (e) $2a''$ HOMO, and (f) $8a'$ LUMO.

At first glance, these two sets of MOs appear unrelated, but a closer inspection indicates that they are actually connected as is further exposed in Fig. 3. The key is from the $1\,^4A''$ state where the H_2OO^+ $8a'$ orbital is singly occupied. As shown in Fig. 2(c), the hydrogen atoms are in-phase with one another even if the

FIG. 3. The H_2OO^+ MO occupations for the $X\,^2A'$, $1\,^2A''$, and $1\,^4A''$ states of H_2OO^+ and the $^2A''$ state of $H_2 \cdots O_2^+$ as labeled from the $X\,^2A'$ state.

adjacent atoms have antibonding interactions. Similar σ antibonding but in-phase hydrogen backbonding has been previously shown in the related $1\,^4A''$ state of H_2SS^{+}.[12] This is the same topology as $7a'$ HOMO-1 (H–H σ-bonding orbital) in $H_2 \cdots O_2^+$ shown in Fig. 2(d). Succinctly, the difference between the MOs in H_2OO^+ and $H_2 \cdots O_2^+$ can be described from Fig. 2 where (a), (b), and (c) become (e), (f), and (d), respectively. Hence, a spin-flip excitation in the $1\,^4A''$ H_2OO^+ state out of the $7a'$ HOMO into the $8a'$ LUMO would create orbital occupations consistent with the occupations of the $^2A''$ state of $H_2 \cdots O_2^+$ again shown in Fig. 3.

The $1\,^4A''$ state of H_2OO^+ and $^2A''$ $H_2 \cdots O_2^+$ have further commonalities. $\angle$ O–O–X is close between the two at 112.9° and 111.5°, respectively, from Table I. Figure 4 is a $^2A''$ two-dimensional PES scanning over the X–H and O–X bond lengths in this case where $\angle$ O–O–X and O–O are frozen at the optimized $^2A''$ $H_2 \cdots O_2^+$ values. The $H_2 \cdots O_2^+$ minimum is clearly produced, but a second local minimum 31.7 kcal/mol (1.37 eV) above the minimum for the complex is also present. The X–H value (y) is 0.8 Å, and the O–X value (x) is 0.7 Å at this local minimum in Fig. 4. These values are nearly the same as the X–H and O–X bond lengths in $1\,^4A''$ H_2OO^+ indicating that the $^2A'' \leftarrow\,^4A''$ excitation in H_2OO^+ takes place here. The excitation energy is approximated to be 44.3 kcal/mol (1.92 eV
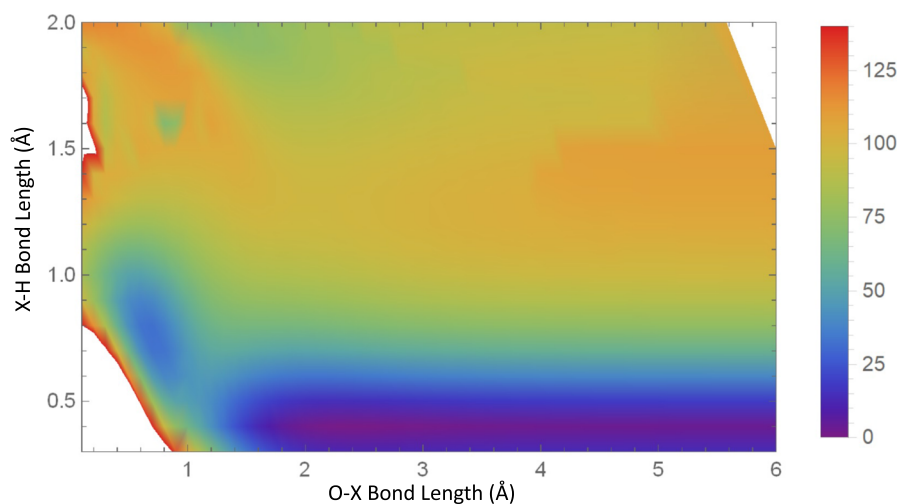
FIG. 4. The $^2A''$ $H_2\cdots O_2^+$ 2D PES with energy gradations in kcal/mol.

or 645 nm) in this region since, again, $1\,^4A''$ H_2OO^+ and $^2A''$ $H_2\cdots O_2^+$ are separated by 12.6 kcal/mol. Additionally, a saddle point between these two minima at X–H = 0.6 Å and O–X = 1.1 Å lies 46.0 kcal/mol (1.99 eV) above the $H_2\cdots O_2^+$ minimum.

Hence, the $1\,^4A''$ state of H_2OO^+ and the $^2A''$ $H_2\cdots O_2^+$ state could interact in the region where the blue second minimum in Fig. 4 occurs. This $^2A'' \leftarrow\,^4A''$ excitation appears to take place in the red of the visible spectrum clearly within the wavelengths of sunlight. Other $H_2\cdots O_2^+$ minima have also been localized in this study, but their X–O bond distances are greater than 4.0 Å. In order to fully characterize any transition from H_2OO^+ into $H_2\cdots O_2^+$, spin-flip excited state determinants and electron dynamics computations originating with the $1\,^4A''$ state of H_2OO^+ or a semiglobal 6D PES surface are necessary in future work. However, the local minimum described above is a very promising region to explore the formation of O_2^+ from water in the gas phase.

CONCLUSIONS

The oxywater cation is shown here to be a possible intermediate in the creation of molecular oxygen from water cations and atomic oxygen. The formation of the oxywater cation begins with $O(^3P)$ atoms bonding with water cations to produce $1\,^4A''$ H_2OO^+. Before becoming $X\,^2A'$ or $1\,^2A''$ H_2OO^+, the quartet state may convert to a different $^2A''$ state instead, $H_2\cdots O_2^+$. The minima of $1\,^4A''$ H_2OO^+ and $^2A''$ $H_2\cdots O_2^+$ are only 12.6 kcal/mol apart adiabatically. Furthermore, the lowest $1\,^4A''$ state of H_2OO^+ has a similar geometry to the local minimum on the $^2A''$ PES corresponding to the $H_2\cdots O_2^+$ complex. The approximated $^2A'' \leftarrow\,^4A''$ excitation for H_2OO^+ in this region is 645 nm, and further refinements of this value likely leading to the $H_2\cdots O_2^+$ complex should not shift it out of the range for solar radiation. The resulting complex after excitation and crossing a low-lying saddle point is then easily dissociated into molecular hydrogen and molecular oxygen. Consequently, the oxywater cation and its $H_2\cdots O_2^+$ complex give all indication of facilitating the creation of molecular oxygen. This has application to various natural processes ranging from the creation of surprisingly high amounts of molecular oxygen in the coma of comet 67P/Churyumov-Gerasimenko

observed during the *Rosetta* mission[13] to the provenance of oxygen on the early Earth potentially including the "snowball Earth" epoch and even to oxygen generation in the upper atmosphere where climate change is driving more water vapor into the stratosphere where it can ionize and react with known atomic oxygen.

COMPUTATIONAL DETAILS

All relative energies and PES scans employ the CCSD(T)-F12/cc-pVTZ-F12 level of theory, except where MRCISD(+Q)/aug-cc-pVTZ is noted. In either case, the MOLPRO2015.1 quantum chemistry program[14,15] is solely utilized. All geometry optimizations are followed by harmonic vibrational frequency computations to ensure that the structures examined are minima and to provide the harmonic zero-point vibrational corrections which are included in the relative energy determinations. The PES scans have displacements of 0.1 Å for the O–O bond lengths (Fig. 1), 0.2 Å for the O–X bond lengths (Fig. 4), and 0.1 Å displacements for the X–H bond lengths (Fig. 4).

SUPPLEMENTARY MATERIAL

The supplementary material contains the MRCISD(+Q)/aug-cc-pVTZ data as a scan of states for the O–O bond elongation.

REFERENCES

[1] B. R. Westbrook, K. M. Dreux, G. S. Tschumper, J. S. Francisco, and R. C. Fortenberry, Phys. Chem. Chem. Phys. **20**, 25967 (2018).

[2] J. M. Hollis, E. B. Churchwell, E. Herbst, and F. C. de Lucia, Nature **322**, 524 (1986).

[3]C. Meredith, T. P. Hamilton, and H. F. Schaefer III, J. Phys. Chem. **96**, 9250 (1992).

[4]Y. Xie, W. D. Allen, Y. Yamaguchi, and H. F. Schaefer III, J. Chem. Phys. **104**, 7615 (1996).

[5]J. Franz, J. S. Francisco, and S. D. Peyerimhoff, J. Chem. Phys. **130**, 084304 (2009).

[6]T. B. Adler, G. Knizia, and H.-J. Werner, J. Chem. Phys. **127**, 221106 (2007).

[7]G. Knizia, T. B. Adler, and H.-J. Werner, J. Chem. Phys. **130**, 054104 (2009).

[8]H.-J. Werner and E.-A. Reinsch, J. Chem. Phys. **76**, 3144 (1982).

[9]T. H. Dunning, J. Chem. Phys. **90**, 1007 (1989).

[10]K. P. Huber, G. Herzberg, J. W. Gallagher, and R. D. Johnson III, in *Constants of Diatomic Molecules*, edited by P. J. Linstrom and W. G. Mallard (National Institute of Standards and Technology, Gaithersburg MD, 2018), p. 69.

[11]R. C. Fortenberry and S. R. Gwaltney, ACS Earth Space Chem. **2**, 491 (2018).

[12]R. C. Fortenberry, T. Trabelsi, and J. S. Francisco, J. Phys. Chem. A **122**, 4983 (2018).

[13]A. Bieler, K. Altwegg, H. Balsiger, A. Bar-Nun, J.-J. Berthelier, P. Bochsler, C. Briois, U. Calmonte, M. Combi, J. De Keyser, E. F. van Dishoeck, B. Fiethe, S. A. Fuselier, S. Gasc, T. I. Gombosi, K. C. Hansen, M. Hässig, A. Jäckel, E. Kopp, A. Korth, L. L. Roy, U. Mall, R. Maggiolo, B. Marty, O. Mousis, T. Owen, H. Rème, M. Rubin, T. Sémon, C.-Y. Tzou, J. H. Waite, C. Walsh, and P. Wurz, Nature **526**, 678 (2015).

[14]H.-J. Werner, P. J. Knowles, G. Knizia, F. R. Manby, M. Schütz, P. Celani, W. Györffy, D. Kats, T. Korona, R. Lindh, A. Mitrushenkov, G. Rauhut, K. R. Shamasundar, T. B. Adler, R. D. Amos, A. Bernhardsson, A. Berning, D. L. Cooper, M. J. O. Deegan, A. J. Dobbyn, F. Eckert, E. Goll, C. Hampel, A. Hesselmann, G. Hetzer, T. Hrenar, G. Jansen, C. Köppl, Y. Liu, A. W. Lloyd, R. A. Mata, A. J. May, S. J. McNicholas, W. Meyer, M. E. Mura, A. Nicklass, D. P. O'Neill, P. Palmieri, D. Peng, K. Pflüger, R. Pitzer, M. Reiher, T. Shiozaki, H. Stoll, A. J. Stone, R. Tarroni, T. Thorsteinsson, and M. Wang, MOLPRO, version 2015.1, a package of *ab initio* programs, 2015, see http://www.molpro.net.

[15]H.-J. Werner, P. J. Knowles, G. Knizia, F. R. Manby, and M. Schütz, Wiley Interdiscip. Rev.: Comput. Mol. Sci. **2**, 242 (2012).